TOP (2015) 23:369–385
DOI 10.1007/s11750-014-0344-x

ORIGINAL PAPER

# Skeletonization for isocentre selection in Gamma Knife® Perfexion™

**Evgueniia Doudareva · Kimia Ghobadi · Dionne M. Aleman · Mark Ruschin · David A. Jaffray**

Received: 21 February 2013 / Accepted: 29 July 2014 / Published online: 20 August 2014
© Sociedad de Estadística e Investigación Operativa 2014

**Abstract** Gamma Knife® Perfexion™ (PFX) is used for delivering radiosurgery plans to treat lesions and tumours in the brain by means of selectively ionizing the tissue with high-energy beams of radiation. An important component of designing PFX treatments is the selection of points in the target structure at which to focus the radiation, called isocentres. This study applies skeletonization methods to select such isocentres. Our skeletonization technique identifies clusters of each target structure's skeleton using distance coding methods. A user-defined number of isocentre locations are chosen from the skeletal clusters. The isocentres resulting from this approach are used as input to a sector duration optimization model that determines the optimal shot shapes and intensities for the radiation deposited at each isocentre. The results for seven clinical cases are presented. For each case, target structure dose and conformity meet clinical radiosurgery guidelines, while brainstem dose is kept to acceptable levels and other healthy organs are also spared.

**Keywords** Skeletonization · Distance coding · Isocentre · Radiosurgery · Gamma Knife Perfexion

E. Doudareva · D. M. Aleman · K. Ghobadi (✉)
Department of Mechanical and Industrial Engineering, University of Toronto,
5 King's College Road, Toronto, ON M5S 3G8, Canada
e-mail: kimia@mie.utoronto.ca

M. Ruschin · D. A. Jaffary
Radiation Medicine Program, Princess Margaret Hospital, Toronto, Canada

M. Ruschin · D. A. Jaffary
Department of Radiation Oncology, University of Toronto, Toronto, ON, Canada

*Present Address:*
M. Ruschin
Odette Cancer Centre, 2075 Bayview Avenue, T Wing, Room TG 217,
Toronto, ON M4N 3M5, Canada

**Mathematics Subject Classification** 90C90 · 90C59 · 90C20

## 1 Introduction

More than 30,000 patients worldwide undergo radiosurgery treatments every year (Elekta 2008). During radiosurgery treatments, a large amount of radiation is deposited into tumours or lesions with an emphasis on conformal dose distributions, that is, dose that tightly follows the contours of the targeted brain tumours or lesions; these targets are called gross tumour volumes (GTVs). High conformality of dose in radiosurgery allows physicians to deliver a high and precise dose to targeted structures while sparing the surrounding healthy tissues, thus improving the patient's survival and quality of life after treatment.

Many studies have focused on the application of radiosurgery to brain cancers for various cancer types often characterized by smaller tumours and multiple lesions (Flickinger et al. 1994, 1990; Petti et al. 2008; Serizawa 2009; Young 1998). Results indicate that compared to traditional open surgery, use of a high precision device, such as Gamma Knife® (Elekta, Stockholm, Sweden), significantly increases patient survival rates (Young 1998). However, there exist variabilities in treatment outcomes that are mostly contributed to the planner's experience and expertise with the machine (Das et al. 2008; Nelms et al. 2012). This variability can be improved through inverse planning, that is, automated planning based on mathematical optimization models (Ferris et al. 2001; Shepard et al. 2003; Wu et al. 2003a).

In Gamma Knife®, several beams are directed at a single point in the patient, called an *isocentre*. While the size of the beam, and whether it is on or off, can be controlled through collimators, earlier models of Gamma Knife® required manual manipulation of the collimators to achieve changes in the beams. Thus, the complex plans obtained through inverse planning methods could not be implemented clinically due to the significant time and effort required to change collimator configurations.

The newest model of Gamma Knife® machines, called Perfexion™ (PFX), improves upon the previous models through automated collimator size selection and couch movement. In PFX, the beams are emitted from eight equi-spaced sectors, and each sector has three collimator sizes (4, 8, and 16 mm) with which to irradiate the patient; these collimator sizes represent beam diameters. The automation of beam size changes and couch positioning allows for complex plans to be delivered clinically, and therefore mathematical models to performed inverse planning are now clinically relevant and useful tools.

Little research has been done in applying mathematical models to PFX treatment planning. Given a fixed set of isocentres, methods to determine the optimal amount of time to deliver radiation from each beam at each possible beam size (called sector duration optimization, SDO) have been presented (Ghaffari et al. 2010; Oskoorouchi et al. 2011; Ghobadi et al. 2012). In (Ghaffari et al. 2010) and (Oskoorouchi et al. 2011), the isocentres used were selected either manually or randomly, and while a hybrid of grassfire and sphere-packing algorithm was employed to find the isocentres in (Ghobadi et al. 2012), the skeleton of the target volumes (a thin medial axis of the volume) was not considered directly. Here, grassfire refers to a method for computing

the distance from a pixel to the border of a specific region. It can be described as "setting fire" to the borders of an image region to yield descriptors such as the region's skeleton or medial axis (Blum 1967). Sphere-packing refers to the type of algorithm that aims at solving the problem of finding an arrangement in which the spheres fill as large a proportion of the space as possible (Ghobadi et al. 2012; Wang 1999).

One of the key decisions within the context of designing treatment plans for Gamma Knife® is the selection of quality isocentre locations inside the target volume (Flickinger et al. 1994, 1990), as choosing well-placed isocentres may significantly improve the dose conformity of the treatment. Finding the best isocentre locations, however, is NP-hard and requires solving a very large mixed-integer optimization problem with binary isocentre location variables and continuous variables for beam durations. In forward planning, a planner has to solve this problem manually. Given the complex nature of the problem and the many decisions that the planner faces, the task is time-consuming and the probability of finding an optimal solution is very low. In inverse planning, exact and heuristic methods are used to find a quality solution to the NP-hard problem, and since inverse planning is independent of planners, it also provides standardization in planning. Furthermore, developing a specific isocentre selection strategy is preferable to random selection, as isocentre positioning affects healthy tissue dosage as well as target coverage (Flickinger et al. 1990).

Skeletonization methods for Gamma Knife® have been previously studied in the literature (Ferris et al. 2001; Shepard et al. 2003, 2008; Wu et al. 2003a; Wu and Bourland 2000; Zhang et al. 2003). In general, skeletonization techniques aim to extract an object's skeleton, which is the object's most basic representation that retains that object's morphology. In shape analysis, a skeleton is a representation of the shape that contains all information that is necessary for reconstructing the original object (Blum 1967). The field of image processing offers a variety of methods for skeleton extraction, depending on the computational complexity of the algorithms and underlying data structure size (Tran and Shih 2005; Molinari et al. 2010; Klette 2007; Bucksch et al. 2010; Lohou and Dehos 2010; Siddiqi and Pizer 2008; Calabi and Harnett 1968; Montanari 1969; Arcelli et al. 1975; Herbin et al. 1996; Preteux 1992). However, these methods are concerned with preserving the skeleton's connectivity and also with retaining the ability to reconstruct the original image. One of the skeletonization techniques that has been explored is "skeleton by influence zones" (SKIZ) algorithm (also known as Voronoi diagram) (Preteux 1992; Herbin et al. 1996). SKIZ is similar to the approach that we aim to take in its attempt to identify the "deepest" clusters at every algorithm iteration based on the assumption that the clusters are the minima of the space. Like in SKIZ, the "skeleton" that we aim to extract from the object is the set of all clusters from all algorithm iterations. However, there are a number of differences between SKIZ and what we require from our clustering method, which is based on thinning approach. For example, SKIZ aims to partition the entire space. The space is not repartitioned in the next iterations but new sub-partitions are added into the existing regions. Unlike SKIZ, we remove the deepest clusters and re-do distance coding using the new information, which creates depth zones that are inherently different from the previous iteration. Furthermore, SKIZ algorithm focuses on the connectivity of each identified cluster with the nearest region, which is not required in our algorithm. In radiation therapy, neither connectivity nor the ability to reconstruct the original object are essential. Therefore

methods such as grassfire transform [e.g., (Wu et al. 2003a; Wu and Bourland 2000)], minimum distance (Ferris et al. 2001; Shepard et al. 2003, 2008), and other thinning techniques combined with sphere-packing approaches are explored in radiation therapy literature to find appropriate volume skeletons. The skeletonization approach is performed on each target structure, and each structure's skeleton represents possible locations of isocentres. The radiation shots (or spheres) are commonly placed on either the end points or the joints of the skeleton to dynamically pack the target's shape with spheres. This process of shot location and duration selection was not initially paired with a separate dose calculation method (Wu and Bourland 2000). However, a fine-tuning beam weight optimization was later introduced (Wu et al. 2003a), and finally dose optimizations were added to the process (Shepard et al. 2003, 2008).

While the sphere-packing approach is known to be NP-hard (Wang 1999), it has been shown theoretically that for perfectly symmetric three-dimensional targets, for instance a spherical target, the sphere-packing solution can be far from the optimal (Wang 2000). This lack of an acceptable set of candidate isocentres likely contributed to poor classical dose conformity indices of 1.17–2.2 (Shepard et al. 2003, 2008; Wu et al. 2003a; Zhang et al. 2003), and attempts to improve these values resulted in further underdosing of the target volume (Shepard et al. 2003). The classic conformity index is a standard clinical measure of conformity, with an ideal value of 1; and clinically accepted values are generally less than 1.2.

Therefore, an important shortcoming of previous applications of skeletonization is that they do not address the challenge of finding an acceptable skeleton of large symmetrical volumes. For example, naively, the skeleton of a sphere of any size is just a point at the centre of the sphere. In the event of a fairly symmetrical volume, common in radiation therapy, if isocentres are selected from the central skeleton, then all isocentres will be clustered at the centre rather than being distributed throughout the structure. Thus, a traditional skeleton may not provide an appropriate candidate set of isocentres. Another shortcoming of previous isocentre selection investigations is the lack of consideration of organs-at-risk (OARs) in the plans (Shepard et al. 2003, 2008; Wu et al. 2003a; Zhang et al. 2003), which can result in overdose of surrounding OARs.

Based on the assumption that every skeletal cluster is positioned at the deepest layer of the target starting from the target boundary, we identified that a cluster of skeletons provide reasonable candidate isocentres for dose delivery. We therefore devise an extension to traditional skeletonization approaches that returns a series of "skeletal clusters" that capture the entire target shape, rather than a simple skeleton; sparing of OARs is then explicitly considered and presented in the SDO phase. We define skeletal clusters as groups of voxels (volumetric cubes representing patient tissue) that are positioned at the deepest levels of the structure when accounting for previously-identified structures. Isocentres are selected from these skeletal clusters. The total number of isocentres in the plan is provided by the user, but the number of isocentres selected from each skeletal cluster is based on the cluster sizes. Once the isocentres are chosen, they are used as input to a previously presented penalty-based SDO model (Ghaffari et al. 2010; Oskoorouchi et al. 2011; Ghobadi et al. 2012) to obtain the optimal sector durations for those isocentres. We tested our isocentre selection approach on seven clinical cases (three of which contain multiple targets). Our results indicate clinically acceptable conformity indices and target coverage values,

that are much improved from previous skeletonization approaches, while sparing all OARs, including the brainstem.

The rest of this paper is organized as follows. Section 2 describes the skeletal cluster approach, as well as an overview of the SDO model. Section 3 presents numerical results tested on four clinical cases, and Sect. 4 contains discussion and conclusions.

## 2 Methods and materials

### 2.1 Skeletal cluster approach

No formal definition of an object's skeleton exists in the literature, however, there are a number of characteristics that are commonly used to define a skeleton (Tran and Shih 2005; Bitter et al. 2001; Klette and Pan 2005; Zhou and Toga 1999):

1. Centredness: The skeleton must be geometrically centred within a structure.
2. Connectivity: The skeleton must have the same level of connectivity as the original structure.
3. Topology: The skeleton must preserve the same topology as the original structure.
4. Thickness: The skeleton must be as thin as possible.
5. Ability to reconstruct the original object.

Given the properties of an object's skeleton, it is reasonable to assume that the skeleton has the capacity to provide an appropriate framework to find a suitable set of isocentre positions, as the skeleton is the most centred structure within the target and therefore isocentres on the skeleton are likely able to reach the entire target with dose. Furthermore, using the skeleton in isocentre selection ensures that the healthy structures neighbouring the target are more likely to be spared during the treatment since the skeleton is centred inside the target.

In the seven cases that we investigated, although the targets vary in size, they all closely resemble a sphere in shape. As previously mentioned, a sphere's true skeleton is simply a dot. Irradiating one point, however, is not desirable, because the dose cannot cover a sufficient fraction of the target volume to allow for effective treatment. Thus, unlike previous skeletonization methods, which we will refer to as "conventional skeletonization methods", that use a single identified skeleton based on the distances from the object's boundary (Ferris et al. 2001; Shepard et al. 2003, 2008; Wu et al. 2003a; Wu and Bourland 2000), we instead define skeletal clusters based on voxel depths, and find multiple clusters within a target, each representing the target's skeleton after every successive iteration. Based on the assumption that every skeletal cluster is positioned at the deepest layer of the target starting from the target boundary, we further deduce that every identified cluster provides reasonable candidate isocentres for dose delivery.

Figure 1a shows the isocentres selected on a synthetic spherical target (with 4.8 $cm^3$ volume) using a conventional skeletonization method and Fig. 1b shows isocentres chosen by our proposed skeletonization for the same target. The concentration of the isocentres at the centre of target in conventional skeletonization methods results in underdose of the target as illustrated by its dose-volume histogram (DVH) in Fig. 2a, while isocentres obtained with the proposed modified skeletonization can produce a

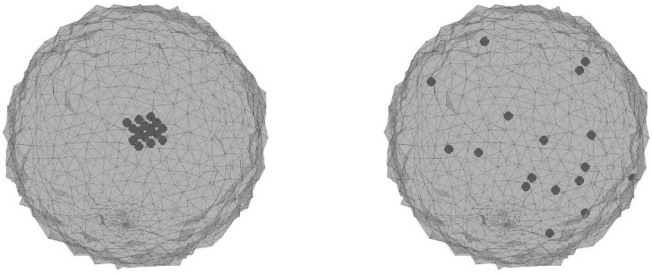

**(a)** **(b)**

**Fig. 1** Isocentre selection on *spherically shaped* target using conventional and modified skeletonization technique. The use of multi-clusters in our proposed method leads to better distribution of the isocentres. **a** Conventional skeletonization, **b** proposed modified skeletonization

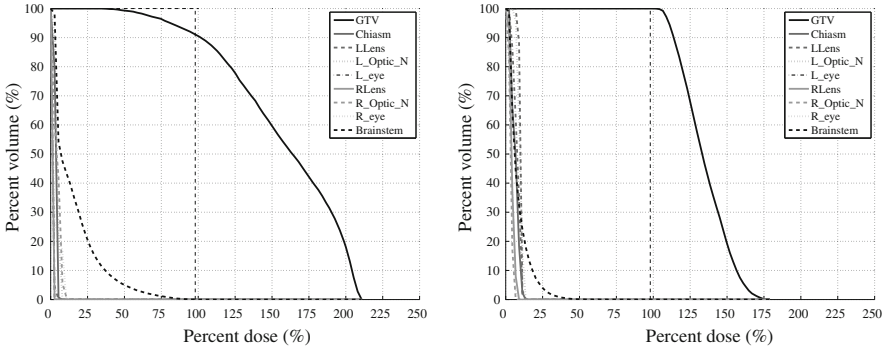


**(a)** **(b)**

**Fig. 2** The dose-volume histogram (DVH) visualizes plan quality based on maximum dose received by percentage volume of different structures. In a DVH, it is desirable that the OARs curves are located towards the *left* of the figure and close to zero and the target curve does not drop until after 100 (indicating that the the entire target received 100 % of the prescribed dose). The DVH figures for plans obtained with isocentres from the conventional and the modified skeletonization techniques show that the modified technique results in better target coverage as well as better healthy organ sparing. **a** Conventional skeletonization, **b** proposed modified skeletonization

conformal plan. For both sets of isocentres, the beam durations were found using an SDO model detailed in Sect. 2.2.

Algorithm 1 provides an overview of our skeletal cluster selection. The algorithm starts with the set of target voxels ($\mathscr{T}$) and a desired number of isocentres ($N$), and returns a quality set of isocentres ($\Theta$) from an appropriate set of clusters ($\Sigma$).

In each iteration of the algorithm, the deepest voxels in the current target volume are considered to be a skeletal cluster. If the volume of the deepest voxels is too small, i.e., less than 1 % of the current target volume, adjacent voxels are also considered as part of the skeleton. This restriction is added to avoid detecting only a few voxels as the skeleton of a large target, which may result in concentration of isocentres in a small area. Once the skeleton is identified, it is subsequently removed from the target (Steps 5 and 6 in Algorithm 1). However, every cluster is only removed for $k$ number of iterations; that is, while the skeletons from the previous iterations are removed, the

skeleton from $k+1$ iterations ago is added back to the target volume (i.e., at each iteration, only the $k$ most recent skeletons are removed from the target) (Step 7 in Algorithm 1) to ensure that future skeletal clusters do not become unacceptably small (see Sect. 2.1.2). A distance coding function ($distCode$) is used to determine which voxels are deepest in the structure by applying an isotropic grassfire algorithm to the current target volume (Sect. 2.1.1). The algorithm runs until all voxels are adjacent to identified clusters or a desired number of clusters is obtained. The grassfire algorithm has been previously used in literature for radiosurgery treatment planning (Ghobadi et al. 2012; Wu and Bourland 2000; Wagner et al. 2000) to find the skeleton of the target volume and also the depth of every voxel in it.

A demonstration of the first four iterations of the algorithm on a representative clinical case (Case 1) is provided in Fig. 3. The colour differences represent the depth of voxel layers relative to the target boundary. In this demonstration, every skeleton is removed from the target for the subsequent two iterations of the algorithm (i.e., $k = 2$). In the first iteration of the algorithm, the deepest voxels are identified as a cluster (labelled as "1" in Fig. 3a). Figure 3b shows the second iteration in which the skeletal cluster "1", that was found in iteration 1, is removed from the voxel set and a new cluster is found (labelled "2"). In the next iteration, a new set of clusters (labelled as "3" in Fig. 3c) are found in the current target, from which both skeletons "1" and "2" are removed. In iteration 4, the cluster from iteration 1 (labelled as "1") is added back to the voxel set, while clusters "2" and "3" (the clusters found in the last two iterations) are removed from the target (Fig. 3d).

Once the skeletal clusters are found, a subset of voxels from each cluster is uniformly selected according to index numbers to be isocentres in the treatment plan (Steps 14–18 in Algorithm 1). The number of isocentres selected from each cluster is proportional to the size of the cluster and the total number of isocentres desired in the treatment plan (provided as user input). Isocentres were not selected from those voxels that are too close to the boundary of the original target volume (in our cases, less than 2 mm

**Algorithm 1** Isocentre selection from skeletal clusters

1: $\mathscr{T} \leftarrow$ set of target voxels; $\Sigma \leftarrow \emptyset$ (set of skeletal clusters, $\Sigma_k$); $N \leftarrow$ desired number of isocentres
2: $distCode \leftarrow$ distance code of all target voxels $v \in \mathscr{T}$
3: $K^{\text{prev}} \leftarrow \emptyset$ (skeletal cluster from previous iteration)
4: **while** $\max(distCode) > 1$ **do**
5: $\quad K \leftarrow \forall v \in \mathscr{T}$ such that $distCode(v) = \max(distCode)$ and $\text{volume}(K) \geq 1\%\ \text{volume}(\mathscr{T})$
6: $\quad T \leftarrow \mathscr{T} \setminus K$
7: $\quad \mathscr{T} \leftarrow T \cup \{S^{k-\text{prev}}\}$
8: $\quad \Sigma \leftarrow \Sigma \cup \{K\}$
9: $\quad K^{\text{prev}} = K$
10: $\quad distCode \leftarrow$ distance code $\mathscr{T}$
11: **end while**
12: $t \leftarrow \sum_{j=1}^{|\Sigma|} |\Sigma_j|$ (the total size of all clusters)
13: $\Theta \leftarrow \emptyset$ (set of isocentres)
14: **for** $j \in \{1 \ldots |\Sigma|\}$ **do**
15: $\quad n \leftarrow N(|\Sigma_j|/t)$ (desired number of isocentres from $\Sigma_j$)
16: $\quad I \leftarrow$ selection of $n$ equi-indexed voxels from $\Sigma_j$
17: $\quad \Theta \leftarrow \Theta \cup \{I\}$
18: **end for return** $\Theta$

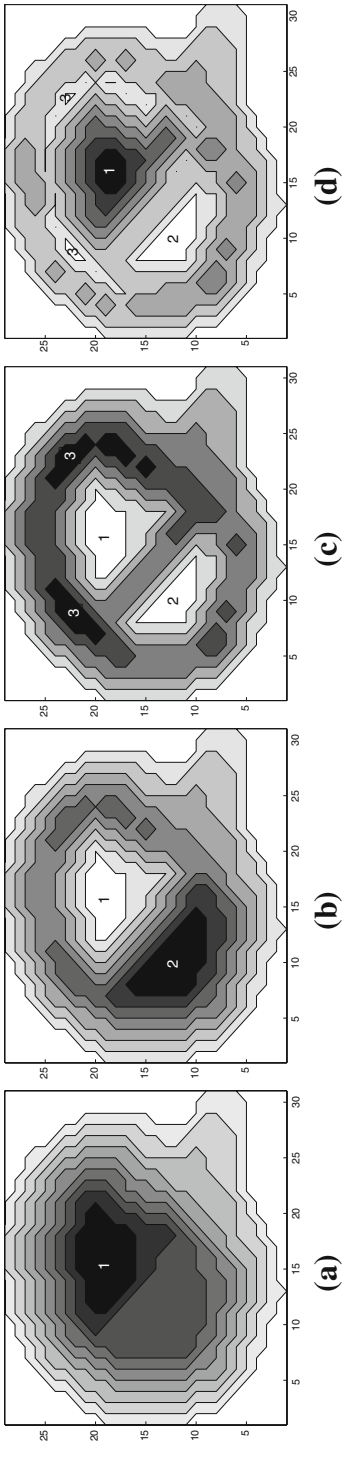


**Fig. 3** The first four iterations of the skeletonization algorithm with $k = 2$ is illustrated for a target cross-section in a representative case (Case 1). In these contour plots, the darkness of the *colour* illustrates the depth of target voxels; *darker coloured* voxels are positioned deeper in the target volume. **a** Iteration 1: the first skeleton is identified (labelled as *1*) in the target. **b** Iteration 2: the skeleton "1" is removed from the current target volume and because $k = 2$ it will not be added back for two iterations (will be added back in iteration 4). The second skeleton is labelled as 2. **c** Iteration 3: The last skeleton (skeleton 2) is also removed from the target for the next two iterations (will be added back in iteration 5). A new skeleton is then found in the current target (labelled as *3*). **d** Iteration 4: The skeleton from three iteration ago is added back (Skeleton 1), while the skeletons from the last two iterations are removed (Skeleton 2 and 3). The algorithm continues in this manner until the desired number of skeletons are reached

distance to the boundary). The minimum distance of the isocentres to the boundary is can be adjusted by the user, if a different distance is desired.

### *2.1.1 Distance coding*

In Algorithm 1, the function $distCode$ is a distance coding metric used to determine the depth of a voxel relative to the target boundary and other skeletal clusters. Our distance metric is based on a grassfire principle (Blum 1967; Arcelli et al. 1975), where the target is represented with artificial unit voxels and then the boundary voxels (voxels having one or more neighbours not in the target) are labelled as having a depth of 1. Target voxels adjacent to boundary voxels are then labelled with increasing integer values layer by layer, until every voxel is assigned a number. The obtained depth for the artificial unit voxels is then used to approximate the depth of the original voxels in the target volume. We use the grassfire principle in our algorithm, because, unlike other distance coding techniques, this method provides us with the means to assess the relative depth of each voxel inside the target from the healthy tissue-target border.

### *2.1.2 Skeletal cluster handling*

Unlike the thinning techniques, our method does not continuously remove layers of voxels to find a medial axis; instead, we aim to identify distinct skeletal clusters by re-using the data from the previous iteration. The data re-insertion helps to better capture the shape of the target by re-using the previously removed voxels to retain the original shape of the target compared to constantly removing voxels that at each iteration shrink the volume of the target. The re-insertion of the previously deleted voxels may also lead to overlapping clusters, and therefore selection of isocentres that are in close proximity of each other. However, hotspots and coldspots are avoided in the treatment plans because the SDO model simultaneously considers all selected isocentres and their possible shot shapes (i.e., various configurations of collimator sizes and beam-on times at each isocentre location).

In this method, in iteration $j$, the deepest distance-coded voxels represent a skeletal cluster ($\Sigma_j$), and are removed from the set of target voxels. The new boundary set includes both the initial boundary voxels, and the voxels neighbouring the removed cluster. All of the remaining target voxels are distance coded against the new boundary set. In the following iteration ($j + 1$), skeletal cluster $\Sigma_{j-1}$ is added back to the boundary set. This approach ensures a selection of isocentres distributed throughout the target. Although in this approach the convergence of the algorithm cannot be guaranteed (due to re-insertion of the previously deleted voxels at each iteration), the algorithm can be terminated after finding a desired number of clusters (a user-defined parameter). In our test cases, we based the required number of clusters on the size of the target volume. We approximately choose one cluster per 1 $cm^3$ of the target volume, except for one of the cases (Case 3) for which we picked more clusters because the shape of the target in this case is the furthest from a sphere among our cases.

## 2.2 Sector duration optimization approach

Although the focus of this study is isocentre selection, our approach to solving the SDO problem, described in (Oskoorouchi et al. 2011; Ghaffari et al. 2010), is presented for completeness. Once the set of isocentres $\mathscr{I}$ is selected, it is fed into the SDO model as input. The SDO method penalizes the amount of underdose or overdose to each voxel, and then attempts to minimize the total penalty in the entire patient by changing beam (collimator) sizes (including turning a beam off) for each of the eight sectors for each isocentre in $\mathscr{I}$.

Let $z_{js}$ be the amount of dose delivered to voxel $j$ in structure $s$, defined as

$$z_{js} = \sum_{i \in \mathscr{I}} \sum_{b \in \mathscr{B}} \sum_{c \in \mathscr{C}} D_{ibcjs} t_{ibc}$$

where $D_{ibcjs}$ is the amount of dose delivered from sector $b \in \mathscr{B}$ with collimator size $c \in \mathscr{C}$ to voxel $j$ in structure $s$ per minute while the couch is positioned at isocentre $i \in \mathscr{I}$, and $t_{ibc}$ is the time in minutes to deliver radiation from sector $b$ with collimator size $c$ to isocentre $i$. The dose to a voxel is then penalized according to the following quadratic penalty function:

$$F_s(z_{js}) = \frac{1}{v_s} \left[ \underline{w}_s \left(T_s - z_{js}\right)_+^2 + \overline{w}_s \left(z_{js} - T_s\right)_+^2 \right]$$

where $T_s$ is the ideal dose delivered to a voxel in structure $s$, $(\cdot)_+$ indicates $\max\{0, \cdot\}$, and $\underline{w}_s$ and $\overline{w}_s$ are penalties for under- and overdosage, respectively. Each voxel penalty is normalized by the total number of voxels in the structure ($v_s$) to ensure that structures do not receive additional consideration based solely on size. In our test cases, a single set of weighting parameters is used for all the cases. In this weighting system, a high weight is considered to ensure conformity of the dose for the target volumes. For our numerical results, we used only one set of weighting parameters for all the clinical cases. In our parameters, large penalties for overdosing the brainstem ($\overline{w}$ = 100 compared to 1 for the rest of the structures) and underdosing the target volume ($\underline{w} = 500$ compared to 0 for the rest of the structures) are considered.

The SDO model is then

$$\begin{aligned}
\text{minimize} \quad & \sum_{s \in S} \sum_{j=1}^{v_s} F_s(z_{js}) \\
\text{subject to} \quad & z_{js} = \sum_{i \in \mathscr{I}} \sum_{b \in \mathscr{B}} \sum_{c \in \mathscr{C}} D_{ibcjs} t_{ibc} && \forall s =\in S,\ j = 1, \ldots, v_s \\
& t_{ibc} \geq 0 && \forall i \in \mathscr{I},\ b \in \mathscr{B},\ c \in \mathscr{C}
\end{aligned}$$

The SDO model is a convex quadratic problem with only non-negativity constraints, and we obtain a solution using the interior-point constraint generation method described in (Ghaffari et al. 2010). In the SDO model, all the structures (including multiple targets in the cases with more than one target volume) are considered and

optimized simultaneously. The dose calculation in SDO is performed using a dose-engine that was provided by the Elekta and models the clinical treatment planning system dose algorithm (TMR10).

## 3 Results

We tested our approach on seven clinical radiosurgery cases (detailed in Table 1) that were obtained with ethical clearance from Princess Margaret Hospital in Toronto, Ontario, Canada. Among our test cases, four targets are acoustic neuromas that impinge upon the brainstem with prescription doses of 12 Gy, and the other three cases are brain metastases (consisting of multiple target volumes) with prescription doses of 24 Gy (over three fractions) and 12 Gy for large tumours (Cases 2 and 4) and small tumours (Case 7), respectively. The target volumes considered among our test cases are all fairly spherical in shape, with the exception of Case 6. Table 1 shows an sphericity measure for each target volume. The sphericity of an object is defined as the ratio of the surface area of a sphere (that has the same volume as the given object) to the surface area of the object (Wadell 1935). Thus, the sphericity of an object with volume $V$ and area $A$ is calculated as $\pi^{1/3}(6V)/A$. The sphericity of a perfect sphere is 1, and sphericity values closer to 1 indicate more spherical objects. The average sphericity

**Table 1** Clinical cases specifications and treatments

| Case | Indication | $V_{100}$ | Voxel vol. ($cm^3$) | GTV vol. ($cm^3$) | # of GTV voxels | Total # of voxels | Sphericity |
|---|---|---|---|---|---|---|---|
| 1 | AN | 98 | 1.2 | 8.56 | 7,178 | 49,538 | 0.78 |
| 2a | MM | 99 | 0.5 | 17.72 | 57,736 | 129,857 | 0.81 |
| 2b | | 99 | | 11.71 | | | 0.69 |
| 3 | AN | 96 | 0.3 | 1.28 | 3,788 | 27,910 | 0.69 |
| 4a | MM | 100 | 0.4 | 0.85 | 77,936 | 125,605 | 0.81 |
| 4b | | 99 | | 25.81 | | | 0.76 |
| 4c | | 100 | | 5.66 | | | 0.89 |
| 5 | AN | 100 | 1.0 | 5.08 | 5,037 | 47,542 | 0.77 |
| 6 | AN | 98 | 2.4 | 13.06 | 13,159 | 47,296 | 0.35 |
| 7a | MM | 98 | 0.6 | 0.19 | 4,945 | 40,369 | 0.65 |
| 7b | | 97 | | 2.71 | | | 0.75 |
| Mean | – | 98.5 | 1.2 | 8.42 | 24,250 | 66,874 | 0.72 |
| St. dev. | – | 1.3 | 2.3 | 8.05 | 30,517 | 49,219 | 0.14 |

*AN* acoustic neuroma. *MM* multiple metastases

index in our test cases was 0.72, with three targets having an sphericity value of greater than 0.8.

Isocentres selected by our skeletal cluster algorithm were fed into the SDO model described in (Oskoorouchi et al. 2011; Ghaffari et al. 2010) to obtain optimal shot shapes and durations. Isocentre selection and SDO were executed on 64-bit Matlab R2009b (The Mathworks, Inc.) for Mac OS X Version 10.6.6 with a 2.53 GHz Intel Core 2 Duo Processor and 4 GB Memory.

In our test cases, the voxels in the targets and the OARs are independent and clinical guidelines for each structure are given. The clinical radiosurgery guidelines require that at least 98 % of each target volume receives 100 % prescribed dose, i.e., $V_{100} \geq 98$ %, while the target dose should not exceed twice of the prescription dose. Additionally, it is required that the maximum dose to any 1 $mm^3$ of the brainstem should be less than 15 Gy. Furthermore, the treatment plans must enable the irradiation of the target in an extremely conformal manner, which is described by conformity indices. A conformity index is a measure of how well the volume of a radiosurgical dose distribution conforms to the size and shape of a target volume (Paddick 2000). The classic conformity index, PIV/TV where PIV is the prescription isodose volume and TV is the target volume, and the Paddick conformity index, $TV_{PIV}^2/(PIV \times TV)$ where $TV_{PIV}$ is the target volume covered by the prescription dose (Paddick 2000; Wu et al. 2003b), must have clinically acceptable values. The classic CI reports the the ratio between the volume that receives the prescribed dose and target's volume, and has values $[0,\infty)$ with

**Table 2** Skeletal cluster algorithm performance

| Case | # Clusters | # Isocentres | Cluster alter. # ($k$) | Skeletonization time (min) | Total comp. time (min) |
|---|---|---|---|---|---|
| 1 | 8 | 20 | 4 | 0.5 | 13 |
| 2 | 11 | 40 | 5 | 3 | 185 |
| | 11 | 40 | 4 | | |
| 3 | 6 | 20 | 2 | 0.5 | 18 |
| 4 | 3 | 3 | 2 | 3.9 | 120 |
| | 18 | 40 | 4 | | |
| | 10 | 20 | 4 | | |
| 5 | 7 | 20 | 5 | 0.4 | 23 |
| 6 | 5 | 45 | 5 | 0.5 | 39 |
| 7 | 3 | 10 | 3 | 0.4 | 34 |
| | 8 | 30 | 4 | | |
| Mean | 8.2 | 26.2 | 3.82 | 1.3 | 61.7 |
| St. dev. | 4.1 | 13.8 | 1.08 | 1.5 | 65.4 |

an ideal value of 1 (clinically acceptable values are 1.3 and lower). The Paddick CI considers both the volume size as well as how much of the irradiated volume was the target volume and has values [0,1], also with an ideal value of 1 (clinically acceptable values are low-0.70s and higher).

Table 2 summarizes computational information about the skeletonization algorithm. Total computation time includes the time required to run the skeletal cluster algorithm plus SDO. Due to the differences in number of target voxels in each case, the number of generated skeletal clusters and the number of iterations $k$ before adding back the clusters to the current volume varies from case to case. The number of isocentres used is correlated with both the number of target voxels and the targets' proximity to the critical structures. It can be noted, however, that the target sizes did not significantly affect the computation performance of the skeletonization algorithm, which took just a few seconds to run for all test cases.

Table 3 provides a quantitative summary of the treatment plan quality for the clinical test cases using our skeletonization method (Inv) and forward plans (Fwd). For easier comparison, the $V_{100}$ of all the inverse plans were normalized to those of the forward plans (as listed in Table 1). Each target in multi-target cases (Cases 2, 4, and 7) is illustrated in a separate row of the table. For a multi-target case, the isocentres in each target are obtained separately, while the SDO problem is performed simultaneously on all the targets. As the table shows, the plan quality over all the cases is comparable with forward plans with an average Paddick CI of 0.84 in inverse plans compared to

**Table 3** Plan quality summary

| Case | Paddick CI | | Classic CI | | Brainstem dose (Gy) | | BOT (min) | |
|---|---|---|---|---|---|---|---|---|
| | Fwd | Inv | Fwd | Inv | Fwd | Inv | Fwd | Inv |
| 1 | 0.85 | 0.86 | 1.14 | 1.12 | 14.4 | 14.4 | 32 | 98 |
| 2a | 0.84 | 0.89 | 1.17 | 1.10 | | | | |
| 2b | 0.80 | 0.85 | 1.23 | 1.19 | 3.0 | 2.5 | 38 | 85 |
| 3 | 0.81 | 0.81 | 1.15 | 1.05 | 14.6 | 13.1 | 34 | 61 |
| 4a | 0.77 | 0.79 | 1.30 | 1.25 | 1.8 | 1.2 | 25 | 91 |
| 4b | 0.83 | 0.85 | 1.18 | 1.18 | | | | |
| 4c | 0.82 | 0.85 | 1.21 | 1.17 | | | | |
| 5 | 0.82 | 0.84 | 1.20 | 1.19 | 14.2 | 14.2 | 24 | 99 |
| 6 | 0.69 | 0.79 | 1.40 | 1.21 | 14.9 | 14.6 | 61 | 177 |
| 7a | 0.67 | 0.81 | 1.38 | 1.21 | 16.9 | 15.1 | 60 | 95 |
| 7b | 0.91 | 0.89 | 1.07 | 1.08 | | | | |
| Mean | 0.80 | 0.84 | 1.22 | 1.16 | 11.4 | 10.7 | 39.1 | 100.8 |
| St. dev. | 0.07 | 0.04 | 0.10 | 0.06 | 6.22 | 6.11 | 15.4 | 36.0 |

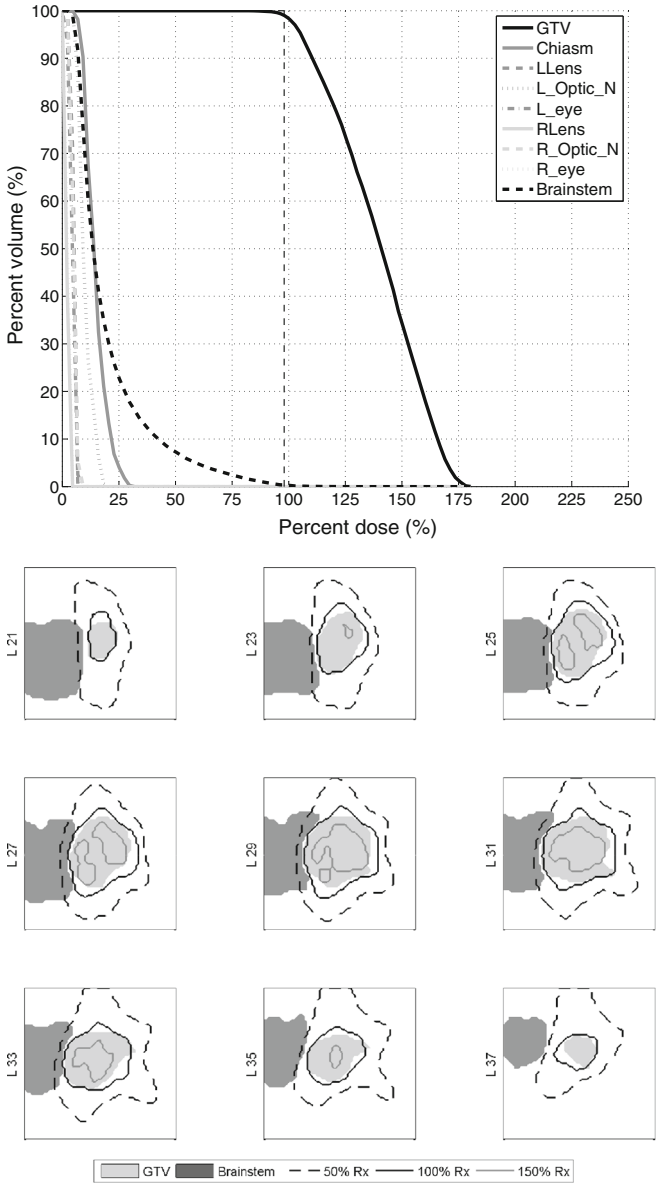


**Fig. 4** *Top* the dose-volume histogram for a representative case (Case 1). This figure shows that 98 % of GTV (*dark solid curve*) received the prescription dose, while only a very small volume of the brainstem (*dark dashed curve*) was irradiated with the full prescription dose, therefore meeting the clinical criteria. The rest of the OARs are all safely located within the first 20 % of the prescription dose, indicating that only a small amount of dose was delivered to them. *Bottom* the isodose lines and isocentre locations shown on cross-sections of the target. The *solid* and the *dashed lines* represents the 100 % and the 50 % isodose lines, respectively

0.80 in forward plans. The average Classic CI in forward and inverse plans is 1.22 and 1.16, respectively. The mean dose to 1 $mm^3$ of brainstem is 11.4 and 10.7 Gy in forward and inverse plans, respectively, however, the dose to brainstem in Case 7 exceeds the clinical guidelines in inverse plans, as it does in the forward plan. The beam-on time was on average much higher in inverse plans with a mean of 101 min compared to an average of 39 min in forward plans.

Dose-volume histograms were also used to assess the quality of the treatment plans. DVHs are plots of the dose received by each percentage of each structure, and are widely used to evaluate radiation treatment plans. Ideally, the target structures should have a DVH curve akin to a step function, with 100 % of the structure receiving 100 % of the prescription dose, and 0 % of the structure receiving more than the prescription dose. As the clinical guidelines indicate, the targets in radiosurgery plans may receive up to 200 % of the prescription dose. Figure 4 provides the DVH and isodose lines for several cross-sections of the target for a representative case (Case 1). These illustrations of the treatment show good conformity, target coverage, and organ sparing.

Our approach obtained clinically acceptable plans for both spherical targets (e.g., target c in Case 4), non-spherical targets (e.g., Case 3) and high irregularity in target's shape (e.g., Case 6). Very large target boundaries with healthy organs (e.g., Case 7 in which two targets are "hugged" by the brainstem) resulted in dose to 1 $mm^3$ brainstem just above the accepted value. These results suggest that our modified skeletonization can be successfully applied to both spherical and irregular targets of any size, however complicated plans with targets with large OARs proximity may be a challenge for our approach.

The computation time for skeletonization algorithm was less than 4 min, while the computation time for the total treatment planning process is on average 62 min. The treatment times for our plans were, however, longer than forward plans by an average of about 61 min. Although the beam-on times were higher than desired, it is important to note that beam-on time was not explicitly considered in either skeletonization algorithm or the SDO model. The largest beam-on time in our test cases belong to the highly irregular target in Case 6 with 177 min, which still produced an acceptable treatment plan quality.

## 4 Conclusions

In this paper, we introduced a new skeletal cluster approach to select quality isocentre locations for radiosurgery treatment planning in PFX. We tested our approach on seven clinical cases with versatile sizes and shapes and achieved better or comparable target conformity than the forward plans. However, plans targets with large brainstem proximity showed lower quality than the rest of the plans. Although this study focused on the application of improved skeletonization to radiosurgery, our skeletal cluster approach could be applied to other fields that traditionally employ skeletonization techniques. The computation time for skeletonization algorithm is under 4 min, while the computation time for the total treatment planning process is around 60 min. The

speed of our approach is especially advantageous when obtaining multiple plans with various clinical criteria is desirable.

Overall, generation of successful treatment plans for the seven clinical cases indicates the versatility of our skeletal cluster approach, as each case offered a unique problem, whether it was the size of the targets, the targets' proximity to healthy tissues, or the number of targets. We tested both spherical and non-spherical tumours, achieving good results in both scenarios. In all cases, clinical treatment guidelines with respect to target dose and organ sparing were achieved. The computation time of our approach was also clinically viable. Although the beam-on times were higher than desired, it is important to note that beam-on time was not explicitly considered in this study because in our clinical guidelines, no restriction on treatment time was given. However, large treatment times are inconvenient for the patients and increase the chances of inaccuracy, for example if the patient moves. Improving beam-on time explicitly in the SDO phase of our inverse treatment planning method is a priority for the future work in this research.

Other future investigations include examining other methods of selecting isocentres from within skeletal clusters, and prioritizing some clusters over others based on, for example, proximity to healthy structures. Although this study focused on the application of improved skeletonization to radiosurgery, our skeletal cluster approach could be applied to other fields that traditionally employ skeletonization techniques, e.g., image processing.

## References

Arcelli C, Cordella L, Levialdi S (1975) A grassfire transformation for binary digital pictures. In: ICPR74-International Conference on Pattern Recognition, pp 152–154

Bitter I, Kaufman A, Sato Y (2001) Penalize-distance volumetric skeleton algorithm. IEEE Trans Vis Comput Graph 7:195–206

Blum H (1967) A transformation for extracting new descriptors of shape. In: Wathen-Dunn W (ed) Models for the perception of speech and visual form. MIT Press, Cambridge, pp 362–380

Bucksch A, Lindenbergh R, Menenti M (2010) SkelTre-Robust skeleton extraction from imperfect point clouds. Visual Comput 26:1283–1300

Calabi L, Harnett W (1968) Shape recognition, prairie fires, convex deficiencies and skeletons. Am Math Mon 75:335–342

Das IJ, Cheng CW, Chopra KL, Mitra RK, Srivastava SP, Glatstein E (2008) Intensity-modulated radiation therapy dose prescription, recording, and delivery: patterns of variability among institutions and treatment planning systems. J Natl Cancer Inst 100(5):300–307

Elekta (2008) Gamma Knife surgery indications treated December 2008. http://www.elekta.com/healthcare-professionals/products/elekta-neuroscience/gamma-knife-surgery/why-gamma-knife-surgery.html

Ferris M, Lim J, Shepard D (2001) An optimization approach for radiosurgery treatment planning. SIAM J Optim 13:921–937

Flickinger J, Lunsford L, Wu A, Maitz A, Kalend A (1990) Treatment planning for Gamma Knife radiosurgery with multiple isocenters. Int J Radiat Oncol Biol Phys 18:1495–1501

Flickinger JC, Kondziolka D, Lunsford LD, Coffey RJ, Goodman ML, Shaw EG, Hudgins RW, Weiner R, Harsh GR, Sneed PK, Larson DA (1994) A multi-institutional experience with stereotactic radiosurgery for solitary brain metastasis. Int J Radiat Oncol Biol Phys 28:797–802

Ghaffari H, Aleman D, Ruschin M, Jaffray D (2010) An inverse planning approach to Leksell Gamma Knife Perfexion. In: Proceedings of the International Conference on the Use of Computers in Radiation Therapy.

Ghobadi K, Ghaffari HR, Aleman DM, Jaffray DA, Ruschin M (2012) Automated treatment planning for a dedicated multi-source intra-cranial radiosurgery treatment unit using projected gradient and grassfire algorithms. Med Phys 39(6):3134–3141

Herbin M, Bonnet N, Vautrot P (1996) A clustering method based on the estimation of the probability density function and on the skeleton by influence zones: application to image processing. Pattern Recognit Lett 17(11):1141–1150

Klette G (2007) Topologic, geometric, or graph-theoretic properties of skeletal curves. Ph.D. thesis, University of Groningen

Klette G, Pan M (2005) Characterization of curve-like structures in 3D medical images. Commun Inf Technol Res Tech Rep 172:164–175

Lohou C, Dehos J (2010) Automatic correction of Ma and Sonkaős thinning algorithm using P-simple points. IEEE Trans Pattern Anal Mach Intell 32:1148–1152

Molinari F, Mantovani A, Deandrea M, Limone P, Garberoglio R, Suri J (2010) Characterization of single thyroid nodules by contrast-enhanced 3D ultrasound. Ultrasound Med Biol 36:1616–1625

Montanari U (1969) Continuous skeletons from digitized images. J ACM 16:534–549

Nelms BE, Robinson G, Markham J, Velasco K, Boyd S, Narayan S, Wheeler J, Sobczak ML (2012) Variation in external beam treatment plan quality: an inter-institutional study of planners and planning systems. Pract Radiat Oncol 2(4):296–305

Oskoorouchi M, Ghaffari H, Terláky T, Aleman D (2011) An interior-point constraint generation method for semi-infinite linear programming with healthcare application. Operat Res 59:1184–1197

Paddick I (2000) A simple scoring ratio to index the conformity of radiosurgical treatment plan. J Neurosurg 93:219–222

Petti P, Larson D, Kunwar S (2008) Use of hybrid shots in planning Perfexion Gamma Knife treatments for lesions close to critical structures. J Neurosurg 109:34–40

Preteux E (1992) Watershed and skeleton by influence zones: a distance-based approach. J Math Imaging Vis 1(3):239–255

Serizawa T (2009) Radiosurgery for metastatic brain tumors. Int J Clin Oncol 14:289–298

Shepard D, Chin L, DiBiase S, Naqvi S, Lim J, Ferris M (2003) Clinical implementation of an automated planning system for Gamma Knife radiosurgery. Int J Radiat Oncol Biol Phys 56:1488–1494

Shepard DM, Yu C, Murphy M, Bussière MR, Bova FJ (2008) Treatment planning for stereotactic radiosurgery. In: Principles and practice of stereotactic radiosurgery, vol 7. Springer Publishing Company, New York, pp 69–90

Siddiqi K, Pizer S (2008) Medial representations: mathematics, algorithms and applications. In: Computational imaging and vision, p 37

Tran S, Shih L (2005) Efficient 3D binary image skeletonization. In: Proceedings of the 2005 IEEE Computational Systems Bioinformatics Conference Workshops (CSBW'05)

Wadell H (1935) Volume, shape and roundness of quartz particles. J Geol 43(3):250–280

Wagner TH, Yi T, Meeks SL, Bova FJ, Brechner BL, Chen Y, Buatti JM, Friedman WA, Foote KD, Bouchet LG (2000) A geometrically based method for automated radiosurgery planning. Int J Radiat Oncol Biol Phys 48(5):1599–1611

Wang J (1999) Packing of unequal spheres and automated radiosurgical treatment planning. J Combinat Optim 3:453–463

Wang J (2000) Medial axis and optimal locations for min-max sphere packing. J Combinat Optim 4:487–503

Wu Q, Bourland J (2000) Three-dimensional skeletonization for computer-assisted treatment planning in radiosurgery. Comput Med Imaging Graph 24:243–251

Wu Q, Chankong V, Jitprapaikulsarn S, Wessels B, Einstein D, Mathayomchan B, Kinsella T (2003a) Real-time inverse planning for Gamma Knife radiosurgery. Med Phys 30:2988–2995

Wu Q, Wessels B, Einstein D, Maciunas R, Kim E, Kinsella T (2003b) Quality of coverage: conformity measures for stereostatic radiosurgery. J Appl Clin Med Phys 4:374–381

Young R (1998) The role of the Gamma Knife in the treatment of malignant primary and metastatic brain tumors. CA Cancer J Clin 48:177–188

Zhang P, Wu J, Dean D, Xing L, Xue J, Maciunas R, Sibata C (2003) Plug pattern optimization for gamma knife radiosurgery treatment planning. Int J Radiat Oncol Biol Phys 55(2):420–427

Zhou Y, Toga A (1999) Efficient skeletonization of volumetric objects. IEEE Trans Vis Comput Graph 5:196–209